

A New Method to Reconstruct the Energy and Determine the Composition of Cosmic Rays from the Measurement of Cherenkov Light and Particle Densities in Extensive Air Showers

A. Lindner

*University of Hamburg, II. Inst.f.Exp.Physik, Luruper Chaussee 149,
D-22761 Hamburg, Germany, E-Mail: lindner@mail.desy.de*

Abstract

A Monte-Carlo study to reconstruct energy and mass of cosmic rays with energies above 300 TeV using ground based measurements of the electromagnetic part of showers initiated in the atmosphere is presented. The shower properties determined with two detector arrays measuring the air Cherenkov light and the particle densities as realized at the HEGRA experiment are processed to determine the energy of the primary particle without the need of any hypothesis concerning its mass. The mass of the primary particle is reconstructed coarsely from the same observables in parallel to the energy determination.

Key words:

Cosmic rays, energy, composition, extensive air showers, air Cherenkov light, HEGRA experiment

PACS: 96.40.De, 96.40.Pq, 13.85.Tp, 13.85.-t

1 Introduction

Despite experimental analyses of charged cosmic rays (CR) since more than 80 years the origin and acceleration sites of CR remain uncertain. A striking feature of the energy spectrum of CR is the so called “knee” around 3 PeV. Below the “knee” the differential energy spectrum follows a simple power law with an index of ≈ -2.7 over an energy range of four orders of magnitude, above the knee the index decreases to ≈ -3.0 and stays roughly constant for the next three orders of magnitude. It is hoped that detailed measurements of

the energy spectrum and the composition of CR around the knee may provide a clue to understand the origin of charged cosmic rays. Possibly the “knee” indicates a transition between two different classes of cosmic accelerators. Contemporary theoretical models describe the acceleration of nuclei in the cosmos mostly by strong shocks [1], either of galactic or extragalactic origin, which can be effectively produced in supernova remnants, supersonic stellar winds, pulsar driven nebulae, active galactic nuclei, relativistic jets in radio galaxies and other phenomena [2].

But neither the acceleration sites could be identified directly by looking for photons resulting from interactions of the accelerated nuclei with the ambient medium, nor were measurements of the charged cosmic rays conclusive. The latter results suffer seriously from the fact, that due to the low flux of CR above 1 PeV only large ground based installations observing the extensive air showers (EAS) induced by cosmic rays in the atmosphere provide experimental data in the energy regime around the “knee”. The sensitivity of EAS observables to the mass of the primary particle is in general rather weak due primarily to large fluctuations of the showers’ developments in the atmosphere which may be larger than mean differences between primary cosmic proton and iron nuclei. The interpretation of experimental data is rendered even more difficult due to theoretical uncertainties concerning high energy interactions in the atmosphere [3,4]. Consequently the experimental results are not conclusive at present and in some cases contradicting to each other (see for example the reviews [5]). Therefore it is highly desired to develop new techniques to measure the properties of cosmic rays between 1 and 10 PeV. Ideally one would combine detailed measurements of the hadronic and muonic shower properties (as performed by the experiment KASCADE [6]) and precise analyses of the development of the electromagnetic shower component, which can be deduced from registered air Cherenkov light for example.

This paper describes a new method to derive the energy spectrum and the elemental composition for energies above a few hundred TeV from measurements of Cherenkov light and particle density at ground level using an experimental setup as realized at the HEGRA installation [7,8]. It will be shown that the energy of a primary particle can be determined independently of its mass with an accuracy of around 10% in the knee region. The mass of the primary particle can be reconstructed coarsely, allowing the determination of the relative amount of light, medium and heavy nuclei in cosmic rays without requiring any hypotheses concerning their energy spectrum. These results will be achieved by analyzing the electromagnetic part of the air shower only. Therefore the new method is complementary to many other results concerning the experimental measurements and the theoretical interpretations of data. Preliminary results of an application of this method to HEGRA data have been presented at conferences ([8,9] and a similar method [10]) proving the validity of this composition analysis by comparison with the results of direct experiments below 1 PeV.

In contrast to earlier analyses of the air Cherenkov light produced in EAS and

results on the development of air showers (see [11] and references therein), this MC study focuses on an interpretation of combined particle and Cherenkov light measurements. A detailed analysis of the Cherenkov light registered relatively close to the shower core is the basis for the energy and mass reconstruction, which can only be improved significantly by adding observables related to the non electromagnetic shower components.

The paper is organized as follows: Next the experimental observables which will be used to reconstruct energy and mass of the primary particle are described. Most important for this analysis are the shape of the lateral Cherenkov light density distribution, the amount of registered Cherenkov light and the number of charged particles at detector level. In the third chapter the event simulation is sketched and features of the longitudinal and lateral shower development in the atmosphere are considered in section four. The following two sections deal with the reconstruction of the position of the shower maximum from the shape of the Cherenkov light density distribution and with an estimation of the energy per nucleon from the penetration depth of the shower until the maximum is reached. In the 7th section the primary energy is derived. Here the shower size at detector level and the known position of the shower maximum are used to determine the shower size at the maximum. This is combined with the energy per nucleon to calculate the primary energy independent of the primary mass. The 8th section presents methods to determine the chemical composition from the observables related to the electromagnetic shower component. Section 9 discusses systematic uncertainties related to the simulation code and estimates the sensitivity of the method presented in this paper to different interaction models. This is followed by a summary and conclusions.

2 The experimental Observables

Although the method presented in this paper was developed primarily for the HEGRA experiment it can equally well be applied to any installation registering air Cherenkov light and charged particles of extensive air showers (EAS). The method can be easily generalized to all experimental setups which allow the determination of the distance to the shower maximum. However some properties of the HEGRA experiment need to be mentioned to understand details discussed in the following sections.

The experiment HEGRA is a multi-component detector complex for the measurement of EAS described elsewhere [7]. At a height of 2200 m a.s.l. it covers an area of 180·180 m². In this paper only the scintillator array of 245 huts on a 15 m grid spacing and the so called AIROBICC array of 77 open photomultipliers sampling the Cherenkov light front of air showers on a 30 m grid spacing are used. Both components feature an increased detector concentration around their common center. The energy threshold (demanding a signal

from at least 14 scintillator or 6 AIROBICC huts) lies at 20 TeV for proton and 80 TeV for iron induced showers.

The measured particle density in the plane perpendicular to the shower axis is fitted by the NKG formula [12]. In the fit a fixed Moliere radius of 112 m is used. The shape parameter *age* and the integral number of particles N_e result from the fitting procedure. As the HEGRA scintillators are covered with 5 mm of lead (which suppresses the detection of low energy electrons but allows the measurement of photons after pair production in the lead) the values obtained for *age* and N_e cannot be compared to simple expectations from the cascade theory.

The Cherenkov light density is analyzed in the interval $20\text{ m} < r < 100\text{ m}$ from the shower core, because the shape of this part of the lateral distribution appears to be independent of the mass of the primary particle (see section 5). In the range between 20 and 100 m the Cherenkov light density can be well described by an exponential

$$\rho_C(r) = a \cdot \exp(r \cdot \text{slope}). \quad (1)$$

Similar to the NKG fit two parameters are obtained from the analysis of the Cherenkov light: the shape parameter *slope* and the total number of Cherenkov photons reaching the detector level between 20 and 100 m core distance, $L(20-100)$.

3 The Generation of the Event Sample

EAS in the energy range from 300 TeV to 10 PeV were simulated using the CORSIKA 4.01 code [13]. The model parameters of CORSIKA were used with their default values and the fragmentation parameter was set to “complete fragmentation”. This results in a complete disintegration of the nucleus after the first interaction. Showers induced by the primary proton, α , oxygen and iron nuclei were calculated. The number of generated Cherenkov photons corresponds to the wavelength interval between 340 and 550 nm. In total 1168 events were generated with CORSIKA 4.01 with zenith angles of 0,15,25 and 35° at discrete energies between 300 TeV and 10 PeV. Systematic comparisons of different event generators to model the interaction of cosmic rays with nuclei of the atmosphere will be sketched in section 9.

In the main this paper assumes perfect measurements of the number of particles and Cherenkov photons and a perfect shower core determination in order to concentrate on the physical principles and limitations of the methods to be described. To study the influence of the realistic experimental performance the events were passed through a carefully checked detector simulation [14] and reconstructed with the same program as applied to the real data. Here each

event was used 20 times to simulate different core positions inside and impact points outside the experimental area, which nevertheless fire a sufficient number of detector huts to fulfill the trigger conditions.

4 The Development of Showers in the Atmosphere

Some basic characteristics of the EAS simulated with CORSIKA 4.01 are summarized here. Features independent as well as sensitive to the mass of the nucleus hitting the atmosphere are described. These will allow the reconstruction of the primary energy and mass from the observables mentioned above.

4.1 *The Shape of the longitudinal Shower Development*

As discussed later in section 5 the shape of the longitudinal shower development behind the shower maximum is most important for the determination of the position of the shower maximum from the lateral Cherenkov light density distribution. Shown on the left of Figure 1 are the mean longitudinal developments of 300 TeV proton and iron induced air showers, where electrons and positrons above an energy of 3 MeV were counted. This will be subsequently called, the shape of the longitudinal shower development. Note that for each shower the maximum (defined as the point in the shower development with the maximal number of particles) was shifted to zero before averaging. Afterwards the mean distribution was normalized to the mean particle number at the shower maximum. With regard to the shape of the longitudinal development behind the shower maximum, no systematic differences depending on the primary particle are visible. The right plot in Figure 1 shows the change in the longitudinal development with increasing primary energy. Independent of the primary particle the longitudinal shower shape becomes more extended behind the shower maximum with rising energy. The independence of the longitudinal shower shape on the mass of the primary nucleus may be explained by a fortunate combination of two effects:

- (1) As visible from simulated proton and iron showers at 300 TeV and 5 PeV the longitudinal shower shape extends with increasing energy (Figure 1, right).
- (2) After the first interaction an iron induced shower can be described as a superposition of nucleon induced subshowers. Each of them has a different subshower maximum position, which fluctuates around a mean value. The longitudinal shape of the whole air shower results from the overlay of all subshowers. Therefore a Fe shower appears to be longitudinally more extended than a proton shower of the same energy per nucleon.

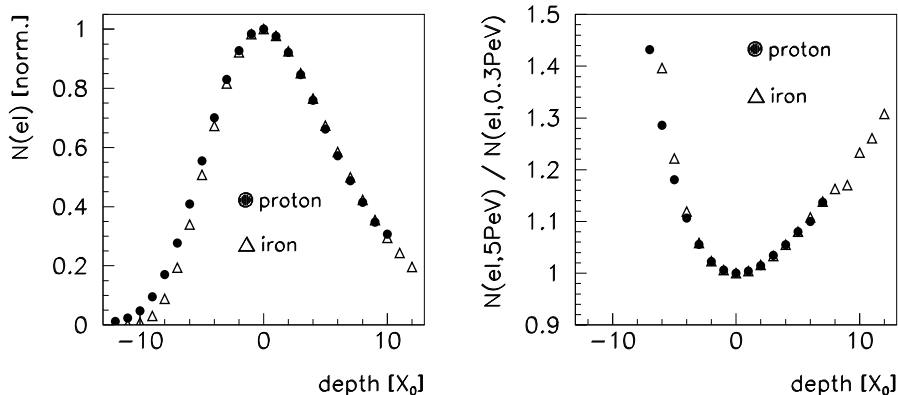


Fig. 1. Left: the mean longitudinal development of 300 TeV p and Fe showers normalized to the number of particles at the maximum. Not that the depth of each individual shower maximum has been shifted to $0 X_0$ before averaging. Right: the ratio of the mean longitudinal development for 5 PeV showers divided by the mean development for 300 TeV showers (normalized at the shower maximum at $0 X_0$).

Both effects combine in such a way that the longitudinal shape of the EAS behind the maximum becomes independent of the mass of the primary nucleon for a fixed primary energy in the simulations used here. This independence is most important for the methods discussed in the following sections. It will allow to determine the distance between detector and shower maximum with the same algorithm for all nuclei.

4.2 The Depth of the Shower Maximum

The mean atmospheric depths of the maxima depend on the energy per nucleon E/A and are subjected to large fluctuations. Figure 2 (left) shows the corresponding correlation: the column density traversed by a shower up to its maximum, named depth of maximum in the following (calculable from the distance and the zenith angle), is correlated equally with E/A for all different simulated primaries from p to Fe and all zenith angles. With the “complete fragmentation” option in our simulations the correlation follows a linear function. From Figure 2 (left) an elongation rate of approximately $82 \text{ g/cm}^2 / \log_{10}(E/E_0)$ is derived:

$$\text{depth(max)} = \left[(335 \pm 3) + (82 \pm 2) \cdot \log_{10} \left(\frac{E/A}{\text{TeV}} \right) \right] \text{ g/cm}^2. \quad (2)$$

If the depth of the shower maximum is measured the energy per nucleon E/A can be inferred, but due to statistical fluctuations of the depth of the shower maxima (Figure 2, right) the resolution for E/A is modest. The fluctuations

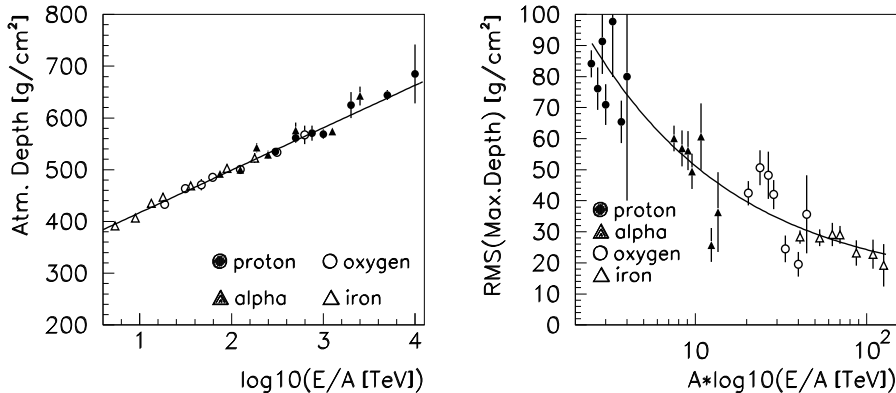


Fig. 2. Left: the mean atmospheric depth of the shower maxima as a function of energy per nucleon. The line shows a fit to the correlation. Right: The fluctuations (rms) of the atmospheric depth of the shower maxima are plotted as a function of energy E and nucleon number A . The line shows a fit to the correlation.

decrease with increasing nucleon number A as the EAS of a complex nucleus consists of many overlapping nucleon induced subshowers so that the whole EAS exhibits less variations than the individual subshowers. The fluctuations diminish slightly also with rising E/A because more interactions take place until the shower maximum is reached. In addition it is interesting to note that for a specific primary particle and energy the number of particles in the shower maximum $N_e(\max)$ does not depend significantly on the depth of the maximum.

The important features used in the following sections are:

- The mean depth of the shower maximum is determined only by E/A .
- Fluctuations in the position of the shower maximum decrease with increasing nucleon number.

4.3 The lateral Shower Development

In hadronic interactions the typical transverse momentum increases only very slowly with rising momentum transfer. Therefore the lateral spread of hadronic showers should decrease with increasing energy per nucleon as the ratio of transverse to longitudinal momentum gets smaller in the early part of the shower development where the energies of the interacting particles are still comparable to the primary energy. In principle this effect could be used as a measure for E/A (if the distance to the shower maximum is known) i.e. by comparing the number of Cherenkov photons reaching the detector level relatively close to the core with all photons detectable at the ground level. In Figure 3 a distinction between heavy and light primaries is obvious at ener-

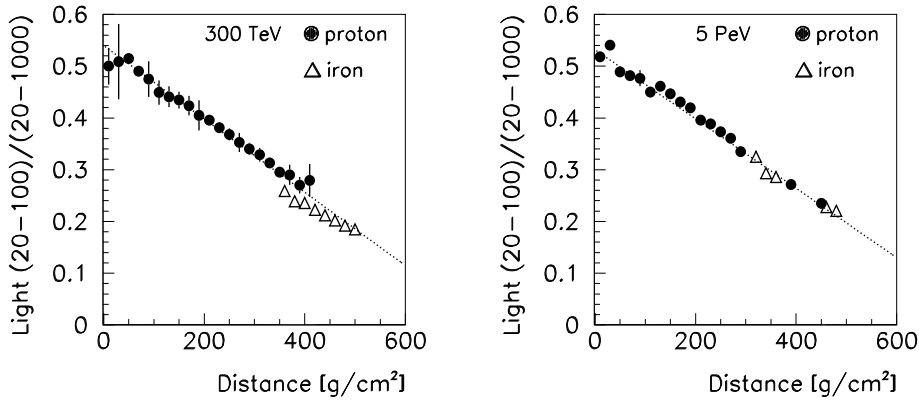


Fig. 3. The mean ratio of the Cherenkov light reaching the detector level between 20 and 100 m core distance to all photons up to 1000 m for 0.3 PeV (left) and 5 PeV (right) iron and proton showers as a function of the distance between detector and shower maximum. The error bars show the rms values of the ratio at a fixed distance, the lines are fits to the correlations for protons to guide the eye.

gies below 1 PeV: iron induced showers are broader than showers of primary protons. However at energies in the knee region nearly no differences between proton and iron showers remain. Obviously here E/A , which determines the longitudinal momentum in hadronic interactions, gets so large even for iron showers that any influence of the hadronic transverse momentum in the first interactions becomes negligible and the lateral extension of the shower is dominated by scattering processes and interactions of particles of lower energies in the later part of the shower development. Qualitatively the same result is achieved by correlating *age* with the distance to the shower maximum. Therefore these features of the lateral shower development can be used only for energies below 1 PeV to enhance the mass sensitivity of EAS measurements in order to improve comparisons with direct balloon data.

5 Reconstruction of the Distance to the Shower Maximum

This section deals with the reconstruction of the distance between the shower maximum and the detector. It will be shown that the distance to the shower maximum can be determined from the shape of the lateral Cherenkov light density with an accuracy of about one radiation length (X_0) at 300 TeV and better than $0.5 X_0$ above 1 PeV.

5.1 The Principle

As already noticed by Patterson and Hillas [15] for proton induced showers with energies above 1 PeV the distance between the detector and the maximum of an EAS can be inferred from the lateral distribution of the Cherenkov light within about 100 m core distance. Simulations with CORSIKA show that this is possible independent of the mass of the primary particle.

The basic ideas of using the lateral extension of Cherenkov light to determine the position of the shower maximum are the following: Cherenkov light emitted at a specific height during the shower development in the atmosphere shows a specific lateral distribution at detector level. The light from the early part of the shower development, where the energies of the particles are still very high so that scattering angles are very small, is concentrated near 120 m (the so called Cherenkov ring at an observation level of 2200 m). Cherenkov light produced closer to the detector level hits the ground closer to the shower core. The measurable Cherenkov light density of the whole EAS is the sum of all contributions from all depth, where lateral distributions from different depths enter with amplitudes corresponding to the number of Cherenkov light emitting particles in the different depths. Hence the shape of the measurable lateral light density distribution depends on the longitudinal shower development. If the shower maximum approaches the observation level more light is produced close to the detector reaching the ground near the shower core. Consequently the lateral Cherenkov light density in the range up to 100 m core distance drops more rapidly, if the shower maximum approaches the detector more closely.

It is important to note that the Cherenkov light in the discussed core distance range is radiated dominantly by particles behind the shower maximum. Therefore the longitudinal shower development behind the maximum determines the correlation between the distance to the shower maximum and the shape of the lateral Cherenkov light density. Figure 4 shows a detailed view of the lateral Cherenkov light distribution for one 300 TeV proton shower. A simple exponential fit can be used to parameterize the distribution between 20 and 100 m core distance (equation 1), although this ansatz cannot account for all details of this distribution. But taking into

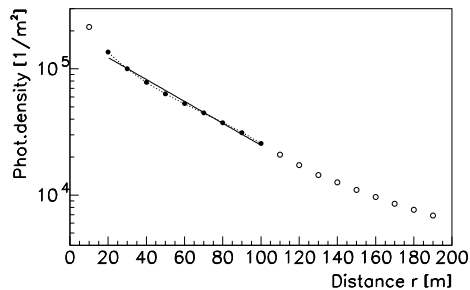


Fig. 4. The lateral Cherenkov light density of one simulated 300 TeV proton shower without experimental uncertainties as a function of the distance to the shower core. Also shown are a fitted exponential (full line, eq. 1) and a function with four parameters (dotted).

account a realistic experimental spread of the light density measurements it is unreasonable to determine more than *slope* and an amplitude parameter in a fit. Therefore just the simple exponential function is used throughout this paper¹.

5.2 The Distance to the Maximum

In Figure 5 the correlation between the distance to the shower maximum and the parameter *slope* derived from the Cherenkov light distribution is plotted for different primary nuclei and zenith angles up to 35° for primary energies of 0.3 and 5 PeV. The distance to the shower maximum can be determined from

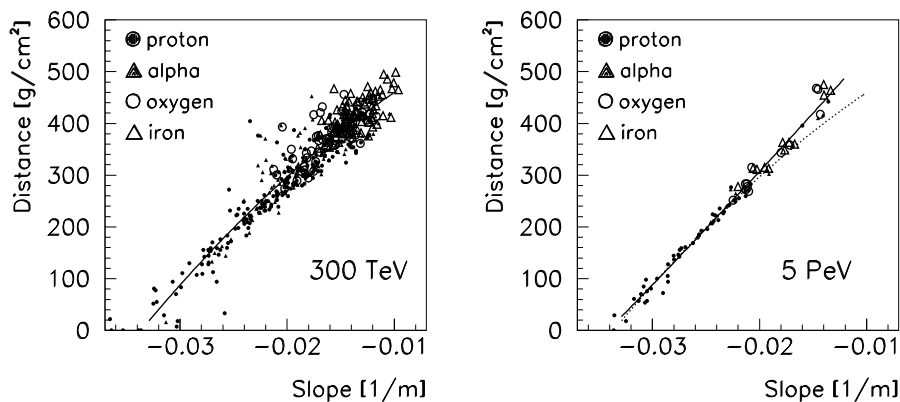


Fig. 5. The distance between detector and shower maxima plotted against the parameter *slope* for 300 TeV (left) and 5 PeV (right) primary energy. The lines show fits to the correlations. The dotted line in the right plot corresponds to the fit to 300 TeV showers to visualize the differences between different primary energies. No experimental uncertainties are considered.

slope independent of the type of the primary particle and zenith angle². The correlation between the distance to the shower maximum and *slope* depends slightly on the primary energy due to the changing longitudinal shower development (see section 4.1). Figure 5 shows simple polynomial fits describing the correlation rather well. The dependence of the fit parameters on $\log(E)$ were again parameterized with polynomials resulting in a two dimensional function of *slope* and $\log(E)$ to determine the distance to the shower maximum. The

¹ If the distance to the maximum is determined using the 4-parameter fit the resolution for the position of the shower maximum compared to the method described below improves by 30% at 300 TeV, whereas no difference in the achievable accuracy was noted above 1 PeV (if no experimental uncertainties are considered).

² neglecting atmospheric absorption

systematic uncertainties in the reconstruction of the distances for primary nuclei from p to Fe and for different primary energies are less than 5% increasing a little for zenith angles of 35° .

The accuracy of the determination of the distance to the shower maximum (for a given primary energy) improves with decreasing distance between detector and shower maximum and with increasing number of nucleons. Both contribu-

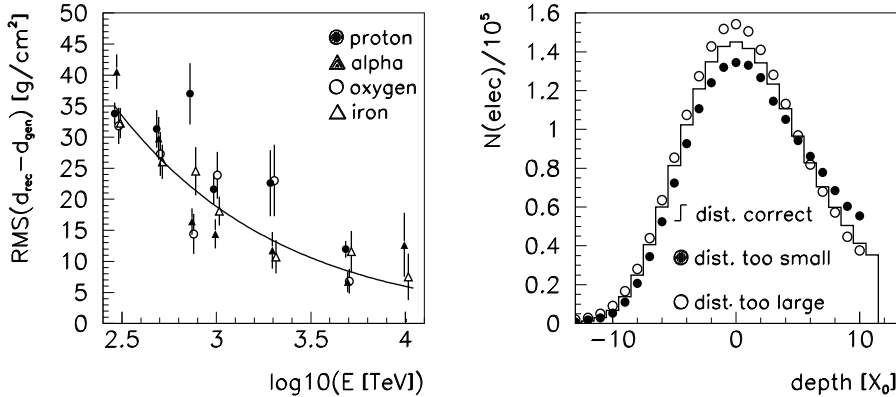


Fig. 6. Left: the rms value of the distributions of the absolute difference between reconstructed (d_{rec}) and MC generated distance (d_{gen}) to the shower maximum for zenith angles of 0° and 15° as a function of energy E . The line shows a fit to the correlation. The rms values increase for larger zenith angles (not shown). Right: the mean longitudinal development of 300 TeV proton showers where the reconstructed distance is more than $20 g/cm^2$ too large (open dots), too small (full dots) or correct within $10 g/cm^2$ (line). The maximum for each individual shower was shifted to zero before averaging. In contrast to Figure 1 the distributions were not normalized to the number of particles in the maximum.

tions compensate such that the resolution averaged over all distances becomes independent of the mass of the primary particle within the statistical errors of the event sample. The resulting precision of the distance determination is plotted in Figure 6 (left) as a function of the primary energy. Fluctuations of the shape of the longitudinal shower development limit the resolution of the distance determination with *slope*, which is shown in the right part of Figure 6. Showers, where the distance is underestimated (overestimated), do not decay as fast (faster) as an average shower behind the shower maximum. Therefore *slope* is smaller (larger) than for the mean longitudinal shower development and the distance is reconstructed too small (large). Figure 6 (right) furthermore proves, that, as expected, the length of the shower behind the maximum is anti correlated with the number of particles in the maximum: the faster the decay after the maximum the more particles arise in the maximum.

Further MC studies show that a method to determine the distance to the shower maximum from the lateral Cherenkov light distribution independent of the mass of the primary nucleus is only possible if the analysis is restricted

to core distances below the so-called Cherenkov ring at 120 m (at an observation level of 2200 m). Extending the analyzed region beyond 120 m introduces a particle dependent bias (compare Figure 3), which however becomes negligible for energies in the region of the knee. Of course other approaches, like the reconstruction of the shower maximum from measurements of the time profile of the Cherenkov light pulses at core distance beyond 150 m [14] show different limitations as different shower properties are measured.

In this section it was shown, that the distance between detector and shower maximum can be derived from the shape of the lateral Cherenkov light density independent of the primary mass. Taking into account a weak dependence on the primary energy a resolution of better than 0.5 radiation lengths is achieved for energies in the knee region.

6 Determination of the Energy per Nucleon E/A

With known distance to the shower maximum and known zenith angle the penetration depth of the shower into the atmosphere until it reaches the maximum can be inferred. The energy per nucleon E/A can be estimated using the correlation shown in Figure 2 (left). In Figure 7 the accuracies of the E/A measurement are shown assuming a perfect determination of the depth of the shower maximum (Fig. 2) as well as deriving the depth from an ideal (Fig. 6) and realistic measurement of *slope*. The uncertainty of the E/A determination for proton induced showers is always dominated by statistical fluctuations of the shower maximum position, whereas for iron showers at low energies the intrinsic uncertainty of the *slope* method contributes significantly. At energies above the “knee” the accuracy is limited by variations of the shower maxima positions for all primary nuclei.

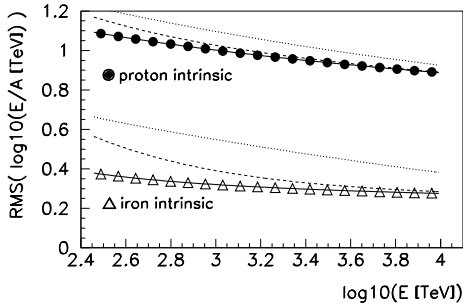


Fig. 7. The accuracy of the E/A reconstruction: “intrinsic” contributions refer to Figure 2 showing the natural fluctuations of the shower maxima positions. The broken lines displays the accuracy achievable with the method to reconstruct the distance to the shower maximum with *slope* assuming perfect measurements of the Cherenkov light densities, the dotted lines shows the results, when a realistic performance of the present HEGRA detector is included (0 and 15° zenith angle).

7 Reconstruction of the primary Energy

The algorithms to reconstruct the primary energy of cosmic rays described in the present paper can be roughly divided into two steps: first the distance of the shower maximum to the detector (derived from the shape of the lateral Cherenkov light density distribution) is combined with the measured number of particles or Cherenkov photons at detector level. In such a way the dependence of these two quantities on different shower maximum distances can be corrected for and an accurate energy determination becomes possible in spite of large natural fluctuation in the position of the shower maxima. Especially the shower size at the maximum $N_e(\text{max})$ will be determined from the shower size at detector level and *slope*.

As only experimental quantities measuring the electromagnetic part of the air shower are considered here it follows naturally, that only the energy deposited in the electromagnetic cascade can be reconstructed directly. In a second step a correction for the non measured energy has to be performed. This correction depends on E/A only, which is determined from the depth of the shower maximum as described in the previous section.

The following plots and parameterizations only take into account showers which reach their maxima at least 50 g/cm^2 above the detector, otherwise one can hardly decide whether a shower reaches its maximum above detector level at all. The treatment of showers arriving at detector level before reaching their maxima has to be considered separately.

7.1 Energy Reconstruction from Particle and Cherenkov Light Measurement

The first step for reconstructing the primary energy is the determination of the number of particles in the shower maximum $N_e(\text{max})$ from the observables N_e and *slope*, because $N_e(\text{max})$ is a good measure of the energy contained in the e.m. cascades. As the scintillator huts of the HEGRA experiment are covered with $1 X_0$ of lead the total number of particles is not measured directly. In simulations the ratio of the number of measured particles and the number of particles incident upon the lead was found to depend only on the distance to the shower maximum but

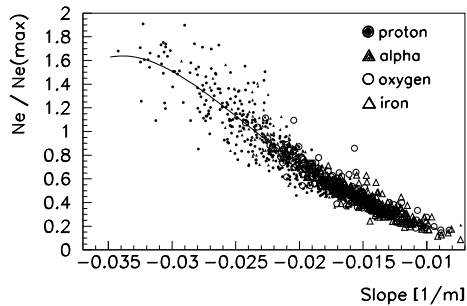


Fig. 8. The ratio of N_e (measured below 0.5 cm of lead) and the number of particles at the maximum $N_e(\text{max})$ as a function of *slope*. The line shows a fit to the correlation, named $\xi_{\text{dis}}(\text{slope})$.

not on the primary energy nor on the nucleon number of the primary particle. Therefore no systematic uncertainties in the shower size reconstruction originate from the lead coverage. The contribution of muons to the number of particles as determined with the NKG fit and the influence of the muons on *age* is less than 1% for the energy range and detector height considered in this paper, provided that the shower core is contained in the detector area of 180 m·180 m. Although negligible the muon component was taken into account when simulating the pulse heights measured by the individual scintillator huts. Due to the conversion of photons in the lead the measured number of particles is larger than $N_e(\max)$ for showers reaching their maximum close to the detector. In Figure 8 the ratio of N_e to $N_e(\max)$ is correlated with *slope* measuring the distance between detector and shower maximum. Using *slope* in this correlation instead of the distance permits the handling of all primary energies in one correlation:

- The function $\xi_{\text{dis}}(\text{slope})$ is fitted to the correlation in Fig. 8 and applied to determine $N_e(\max)$ from N_e at detector level and from *slope*.

No systematic differences between different primary particles were noticed. The shower size at the maximum can be reconstructed from N_e and *slope* with accuracies ranging from 20% (15%) for Fe (p) induced showers of 300 TeV energy to 8% (12%) at 5 PeV. The accuracy for 300 TeV iron showers is limited by the number of fired scintillator huts, whereas the accuracy for primary protons is always limited by fluctuations in their shower development profiles for the energy range and the experimental setup considered here. In the second step the primary energy is determined from $N_e(\max)$ and E/A . Two sub steps are necessary here: first the energy contained in the electromagnetic part of the EAS has to be derived, followed by an E/A dependent correction to determine the primary energy. The electromagnetic energy is proportional to $N_e(\max)$ for a fixed shape of the longitudinal shower development. Because the shape changes slightly with primary energy E an iterative procedure has to be applied to determine E finally. Two functions are defined to determine the primary energy from $N_e(\max)$ and E/A . Note that arbitrary factors may be multiplied to $\xi_{\text{lon}}(E)$ and $\xi_{\text{em}}(E/A)$ below as long as their product is kept constant.

- The function $\xi_{\text{lon}}(E)$ takes into account the change of the longitudinal shower development with E . It was determined from the EAS simulations:

$$\xi_{\text{lon}}(E) = \frac{N_e(\max)}{E \cdot \xi_{\text{em}}(E/A)} = 532 \text{ TeV}^{-1} \cdot \left[1 + \left(\frac{E}{6.62 \text{ TeV}} \right)^{-0.602} \right]. \quad (3)$$

The function varies by 8% between 300 TeV and 5 PeV primary energy.

- The function $\xi_{\text{em}}(E/A)$ is used to derive from the electromagnetic energy and E/A the total energy E of the primary nucleus and will be discussed a little more detailed below.

To determine ξ_{lon} and ξ_{em} in an iterative manner first $\xi_{\text{lon}} \equiv 1$ is assumed and ξ_{em} derived from a fit to the generated events. Afterwards ξ_{lon} is fitted to the correlation of $\text{Ne}(\text{max})/(\text{E} \cdot \xi_{\text{em}})$ versus E , which in turn allows to determine a new parameterization for ξ_{em} . After two iterations neither ξ_{lon} nor ξ_{em} change anymore.

The fraction of the primary energy which goes into the electromagnetic part of the shower (parameterized by ξ_{em}) rises with increasing energy as the probability for hadrons to perform subsequent interaction with the production of additional neutral pions (feeding the em. cascade by their decay to two photons) increases with the hadron energy. For a nucleus the fraction of the electromagnetic energy should depend only on E/A . Following the results of [16] a function was fitted to the correlation of $\text{Ne}(\text{max})/\text{E}$ with E/A using the generated MC events:

$$\xi_{\text{em}}(\text{E}/\text{A}) = \frac{\text{Ne}(\text{max})}{\text{E} \cdot \xi_{\text{lon}}(\text{E})} = \left[1. - \left(\frac{\text{E}/\text{A}}{33 \text{ GeV}} \right)^{-0.181} \right] \text{TeV}^{-1}. \quad (4)$$

The ratio of this correction for proton to iron showers at 300 TeV amounts to 1.34 decreasing to 1.16 at 5 PeV (see Figure 10). These ratios are larger than derived by extrapolating the results in [16] to the mean atomic number of air because the fraction of the total energy deposited in the electromagnetic cascade is different in air showers compared to showers developing in solid state calorimeters: in air the interaction length for charged pions is comparable to their decay length so that the competition between pion decay and secondary interaction with subsequent production of neutral pions lowers the fraction of energy deposited in the electromagnetic cascade.

$\xi_{\text{em}}(\text{E}/\text{A})$ is determined as $\xi_{\text{em}}(\text{maximum depth})$, which is calculated as $\xi_{\text{em}}(\text{slope}, \theta, \text{E})$, where θ denotes the zenith angle. The primary energy enters, because of the small energy dependence of the shape of the longitudinal shower development behind the maximum. Now the primary energy is calculable by

$$\text{E} = \frac{\text{Ne}(\text{max})}{\xi_{\text{lon}}(\text{E}) \cdot \xi_{\text{em}}(\text{E}/\text{A})} = \frac{N_e}{\xi_{\text{dis}}(\text{slope}) \cdot \xi_{\text{lon}}(\text{E}) \cdot \xi_{\text{em}}(\text{slope}, \theta, \text{E})}. \quad (5)$$

Due to the energy dependencies of ξ_{lon} and ξ_{em} , both due to a slightly changing shape of the longitudinal shower development, energy and distance to the shower maximum cannot strictly be determined separately but have to be calculated iteratively. Usually two iterations turn out to be sufficient.

The application of the whole procedure to simulated events results in systematic uncertainties in the order of 5% for the reconstructed primary energy compared to the generated energy (Figure 9). Several contributions to the energy resolution for iron and proton showers are listed in Table 1. For 300 TeV

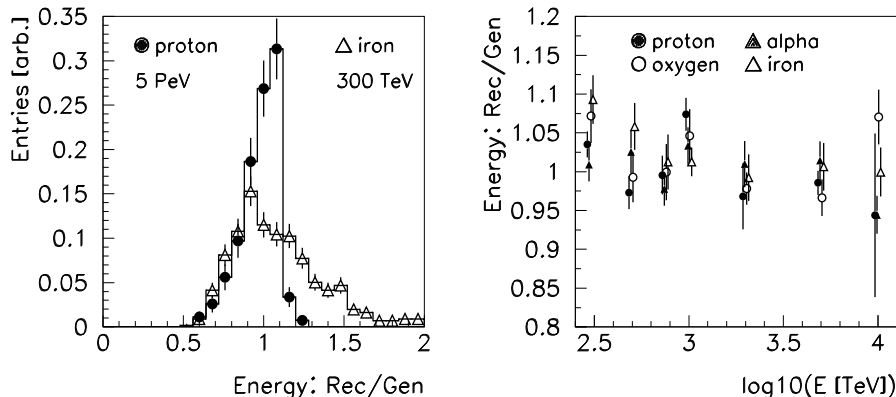


Fig. 9. Left: the ratio of reconstructed and generated energy for 5 PeV proton and 300 TeV iron showers (as two extreme cases for the energy per nucleon in the used event sample). Right: the mean value of the same ratio for different primaries and energies (right). Only events with a minimal distance of 50 g/cm^2 were considered in both plots. Each generated event was used several times with different core positions to take into account the experimental uncertainties for the N_e determination properly.

iron showers most of the uncertainties stem from N_e , determined with the NKG fit to a relatively small number of fired scintillator huts, and from a modest resolution for E/A . For energies of 1 PeV and larger the resolution amounts to roughly 10%. The much improved energy resolution is achieved due to better N_e and E/A determinations and a smaller E/A dependent correction. The energy resolution for proton showers improves from 25% at 300 TeV to about 10% at 5 PeV. Above 1 PeV even a direct measurement of $N_e(\text{max})$ and an unambiguous identification of the proton would not improve the energy resolution very much compared to the reconstruction using only experimental observables.

7.2 Energy Reconstruction from Cherenkov Light alone

Similar to the method described in the previous section the energy can be reconstructed by replacing N_e by $L(20-100)$. A difference arises, because N_e is a good measure of all charged particles produced in e.m. interactions and reaching the detector level, while $L(20-100)$ comprise only about 20% to 60% of all Cherenkov photons at detector level (Fig.3). The fraction of $L(20-100)$ compared to all Cherenkov photons reaching the detector level depends on the distance to the shower maximum like N_e , but in addition it depends on the lateral spread of the air shower. This introduces an additional E/A dependency (besides the E/A dependent fraction of the primary energy deposited in the

Table 1

The energy resolutions achieved by using different parameters, which were taken either directly from the MC generator or reconstructed from the detector information. In the first two rows the identity of the primary particle is used from the simulations. “Ne(max)”, “Ne at detector” and “distance” (the distance between detector and shower maximum) are quantities taken from the MC generator, N_e and $slope$ experimental observables. E/A denotes the energy per nucleon, which in the last line of the table is reconstructed from $slope$ and the zenith angle.

Input Parameters		Energy Resolution (RMS)			
MC gen.	Reconst.	Fe 300 TeV	Fe 5 PeV	Prot. 300 TeV	Prot. 5 PeV
Ne(max)		$(6 \pm 1)\%$	$(4 \pm 1)\%$	$(15 \pm 1)\%$	$(9 \pm 1)\%$
Ne at detector, distance		$(12 \pm 1)\%$	$(6 \pm 2)\%$	$(17 \pm 1)\%$	$(7 \pm 1)\%$
distance	N_e	$(20 \pm 2)\%$	$(7 \pm 2)\%$	$(18 \pm 1)\%$	$(11 \pm 2)\%$
E/A	$N_e, slope$	$(22 \pm 2)\%$	$(7 \pm 2)\%$	$(15 \pm 1)\%$	$(11 \pm 2)\%$
	$N_e, slope$ E/A	$(31 \pm 3)\%$	$(12 \pm 4)\%$	$(25 \pm 2)\%$	$(11 \pm 2)\%$

electromagnetic cascades), because the lateral spread of an EAS decreases with decreasing ratio of transverse to longitudinal momentum in the hadronic interactions. This effect was already discussed in the text related to Fig. 3, while comparing proton and iron showers of the same primary energy. The following effects were taken into account for the energy reconstruction with Cherenkov light only:

- The fraction of Cherenkov light measured in the range of 20 to 100 m core distance $L(20-100)$ compared to all Cherenkov photons reaching the detector level depends on the distance to the shower maximum and in addition on the primary energy due to small differences in the longitudinal shower shapes. Both dependencies were parameterized with the functions $\zeta_{\text{dis}}(slope)$ and $\zeta_{\text{lon}}(E)$ (corresponding to ξ_{dis} and ξ_{lon} of the previous section).
- For a given distance and primary energy the number of all Cherenkov photons contained in $L(20-100)$ depends on E/A. This was parameterized with the function $\zeta_{\text{em}}(E/A)$.
- The threshold for electrons to produce Cherenkov light varies from 55 MeV at a height of 150 g/cm² to 24 MeV at the detector level of 793 g/cm². Therefore the amount of Cherenkov light generated in the atmosphere depends on the height of the shower maximum. This is taken into account with $\zeta_{\text{den}}(\text{height})$.

The correction depending on energy per nucleon is given explicitly below.

$$\zeta_{\text{em}}(E/A) = \frac{L(20 - 100)}{E \cdot \zeta_{\text{dis}} \cdot \zeta_{\text{lon}} \cdot \zeta_{\text{den}}} = \left[1. - \left(\frac{E/A}{178 \text{ GeV}} \right)^{-0.180} \right] \frac{10^7}{\text{TeV}} \quad (6)$$

This correction varies more strongly with E/A than equation 4 because of the discussed additional E/A dependency. Equation 4 and 6 are compared in Figure 10. The remaining systematic uncertainties of the energy reconstruction with Cherenkov light only for different primary particles, energies and zenith angles are less than 10%, a little worse compared to the energy reconstruction with N_e . The reason is the larger E/A dependency. The energy resolution ranges from 45% (35%) at 300 TeV to 8% (11%) at 5 PeV for iron (proton) induced showers. Details are listed in Table 2. By comparing the first two rows of the table one can deduce that the described method contains all relevant corrections which have to be applied for an energy reconstruction. Even optimizing for a specific particle and energy but restricting to Cherenkov light measurements between 20 and 100 m gives no improvement compared to the algorithm of this section. Although $L(20-100)$ can be measured (assuming a perfect detector) with a precision of 1%, which is much better than a determination of N_e with the scintillator array, the final accuracy for the primary energy is even a little worse, if only Cherenkov light is used instead of N_e and *slope*. The final limitation is due to the energy contained in the non electromagnetic shower components, which are not measured here and have to be corrected for via a rather uncertain E/A estimation. The energy determination can only be improved, if the hadronic and muonic EAS components are registered in addition to the discussed setup.

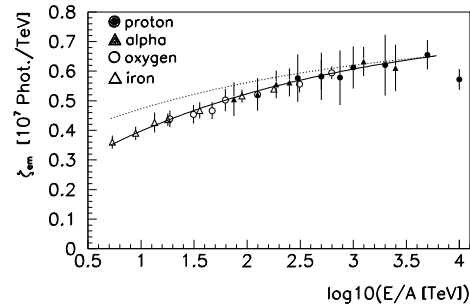


Fig. 10. The energy per nucleon dependent function ζ_{em} (equation 6). The error bars show the spread (RMS) for each energy and primary. The line shows a fit to the correlation. The dotted line corresponds to equation 4 normalized to eq. 6 at 5 PeV.

Table 2

The rms values of the ratio of reconstructed energy (only from Cherenkov light) to generated energy. For all results the observable $L(20-100)$ was used. The first row shows an ideal case, where the energy reconstruction methods were optimized for a special primary particle and MC energy. The following rows list the numbers obtained with the method described in the text, where either MC generated or reconstructed quantities are used. "Distance" stands for the distance between detector and shower maximum.

Input Parameters		Energy Resolution (RMS)			
MC gen.	Reconst.	Fe 300 TeV	Fe 5 PeV	Prot. 300 TeV	Prot. 5 PeV
log(A), distance	$L(20-100)$	$(9 \pm 1)\%$	$(6 \pm 2)\%$	$(15 \pm 1)\%$	$(9 \pm 1)\%$
E/A, distance	$L(20-100)$	$(9 \pm 1)\%$	$(6 \pm 2)\%$	$(15 \pm 1)\%$	$(9 \pm 1)\%$
E/A	$L(20-100),$ $slope$	$(15 \pm 2)\%$	$(6 \pm 2)\%$	$(17 \pm 1)\%$	$(9 \pm 1)\%$
	$L(20-100),$ $slope, E/A$	$(45 \pm 4)\%$	$(8 \pm 3)\%$	$(35 \pm 2)\%$	$(11 \pm 2)\%$

8 Determination of the Chemical Composition

With the reconstruction of the shower properties described in the previous sections not only the energy is inferred independently of the mass of the primary nucleus but also the nucleon number of the hadron hitting the atmosphere can be determined coarsely. In the following sections first a nucleon number estimation derived from the longitudinal shower development will be presented. This procedure will be most important for the analysis of the chemical composition. Secondly the properties of the lateral shower extensions will be analyzed for their sensitivity on the nucleon number of the primary particle. The third section combines all information concerning the chemical composition deduced here from the four observables N_e , age , $slope$ and $L(20-100)$ for 300 TeV showers as an example.

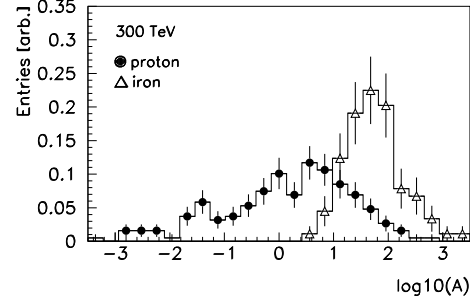


Fig. 11. The reconstructed nucleon numbers for proton and iron primaries of 300 TeV.

8.1 The Chemical Composition from the longitudinal Shower Development

Using the described procedures to determine the primary energy and to estimate the energy per nucleon E/A from the position of the shower maximum as described in section 6 it is straightforward to calculate the nucleon number:

$$\log_{10}(A) \equiv \log_{10} \left(\frac{\text{energy}}{\text{energy/nucleon}} \right). \quad (7)$$

Figure 11 displays the reconstructed $\log_{10}(A)$ values for proton and iron showers of 0.3 and 5 PeV. The other primaries were omitted in order to keep a clear picture. Further results are summarized in Table 3. The reconstructed mean values correspond within statistical errors to the expectation values. For the energy reconstruction the method with N_e was used, but very similar results are obtained with the method using only Cherenkov light to determine the primary energy.

Light and heavy primaries can be distinguished by their different mean values and by their different spreads. The spread of the $\log_{10}(A)$ distributions is dominated by the statistical fluctuations of the depths of the shower maxima with subsequent uncertainties in the E/A determination (see Figures 2 and 7).

Table 3

The mean and rms values of the distributions of the reconstructed $\log_{10}(A)$ values. "Rec." marks the results achieved from the reconstructed energies and energies per nucleon as described in the text. Differences to the fits shown in Figure 7 originate from the summation over all zenith angles in this table. "Gen." symbolizes the results obtained by using the generated MC energy and the depth of the shower maximum directly from the event simulation. The numbers given in the "Gen." columns therefore show the contributions from fluctuations in the longitudinal shower development only. Even a perfect energy determination would hardly improve the separation of different primary particles.

Primary	$\langle \log_{10}(A) \rangle$	RMS of $\log_{10}(A)$			
		300 TeV Rec.	300 TeV Gen.	5 PeV Rec.	5 PeV Gen.
Proton	0.00	1.19 ± 0.09	1.00 ± 0.07	0.82 ± 0.13	0.77 ± 0.12
Helium	0.60	0.83 ± 0.08	0.70 ± 0.07	0.42 ± 0.12	0.30 ± 0.09
Oxygen	1.20	0.63 ± 0.08	0.52 ± 0.07	0.26 ± 0.08	0.22 ± 0.06
Iron	1.75	0.53 ± 0.06	0.35 ± 0.04	0.38 ± 0.11	0.29 ± 0.09

8.2 Composition Analysis from the lateral Shower Development

For energies below the knee region differences concerning the lateral EAS extensions (section 4.3 can be used to distinguish between different primaries, if the energy of the primary particle and the distance to the shower maximum are known. The sensitive parameters are *age* and the fraction of $L(20-100)$ compared to all Cherenkov photons at detector level.

To exploit this the expectation value of *age* for proton induced showers was parameterized as $\text{age}(p) = 1.42 - 0.10 \cdot \log_{10}(E/\text{TeV}) + 18.0 \cdot \text{slope}$. For each reconstructed shower the actual *age* is then compared to the expectation for primary protons. Figure 12 (left) visualizes the distinction between 300 TeV proton and iron induced showers. As expected Fe showers appear to be broader than p showers.

When comparing the number of Cherenkov photons within and beyond 100 m core distance, one encounters a technical difficulty, because it is very problematic to measure the low density Cherenkov light up to a few hundred meters distance from the shower core with great precision. However using the energy reconstruction methods developed in this paper an indirect measurement of the fraction of $L(20-100)$ compared to all Cherenkov photons reaching the detector level is possible: if the energy is reconstructed only with Cherenkov light an E/A dependent correction (eq. 6) has to be applied to take into account the changing fraction of Cherenkov light measurable within 100 m core distance and the fraction of the primary energy deposited in the electromagnetic cascade. Only the latter point has to be corrected for if the energy reconstruction is done with the help of N_e (eq. 4). Therefore omitting all E/A corrections in both energy reconstruction methods (resulting in $E^*(Cl)$ and $E^*(N_e)$) and then comparing $E^*(Cl)/E^*(N_e)$ provides an indirect estimation of the fraction of Cherenkov light beyond 100 m core distance. This is equivalent to comparing the number of Cherenkov photons between 20 and 100 m core distance to N_e taking into account the distance to the shower maximum and density effects for the production of Cherenkov light. In Figure 12 (right) the energy ratios are plotted. A clear separation is visible for 300 TeV showers. Unfortunately at energies in the "knee" region the lateral extensions no longer depend on the primary mass in a measurable way.

8.3 Chemical Composition from a combined Analysis of the longitudinal and lateral Shower Development

The sample of 300 TeV showers was used to compare the sensitivity of the different parameters discussed in the last two sections on the mass of the primary nucleus. If cuts in the $\log_{10}(A)$, $\text{age}/\text{age}(p)$ or $E^*(Cl)/E^*(N_e)$ distributions are applied so that 90% of the iron showers are selected, the following fractions of

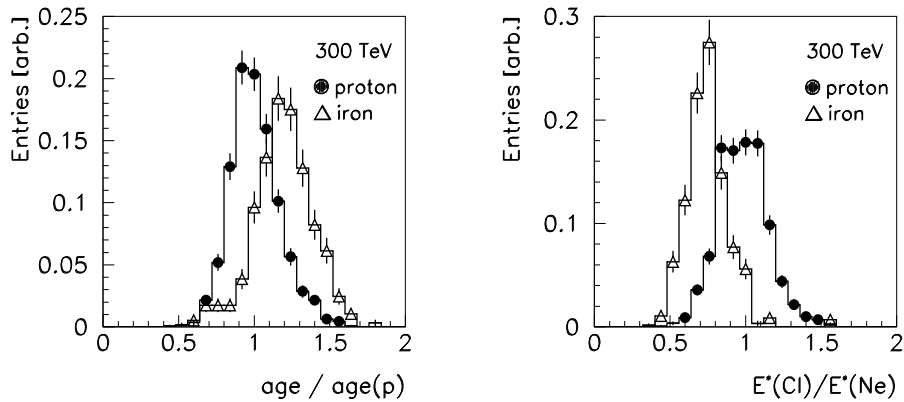


Fig. 12. The age values divided by the expectation value for protons (left), and the ratio of the energies reconstructed only with Cherenkov light and by using N_e and $slope$, where all corrections depending on E/A were omitted (right). Proton and iron showers of 300 TeV are displayed. The simulated showers have been used several times with different core positions to take into account experimental uncertainties related to the NKG fit.

proton showers remain:

- cut in $\log_{10}(A)$: 20%, – cut in $age/age(p)$ or $E^*(Cl)/E^*(N_e)$: 40%.

The most sensitive parameter clearly is derived from the longitudinal shower development. To combine the information from the longitudinal shower development and the lateral extension of the EAS the probability densities, dubbed “ ϱ ” below, for observing a specific $\log_{10}(A)$, $E^*(Cl)/E^*(N_e)$ or $age/age(p)$ value were parameterized for primary p, α , O and Fe nuclei of 300 TeV from the MC library. Following equation 8 (similar for other primaries) a combined probability \mathcal{P} is calculated.

With $\rho_{Fe} = \varrho(\log_{10}(A), Fe) \cdot \varrho(E^*(Cl)/E^*(N_e), Fe) \cdot \varrho(age/age(p), Fe)$:

$$\mathcal{P}(Fe) = \frac{\rho_{Fe}}{\rho_p + \rho_\alpha + \rho_O + \rho_{Fe}} \quad (8)$$

Table 4 lists the fractions for nuclei of different masses which are obtained by selecting 90% or 50% of all proton or iron showers. Clearly an analysis of the chemical composition improves, if measurements of the longitudinal and lateral shower developments are combined at 300 TeV. Light and heavy particles can be separated rather well. With the four observables used here nuclei with masses similar to oxygen can be separated from light and heavy primaries only in a statistical sense but not on an event by event basis. It seems to be difficult to distinguish between primary protons and α particles.

Table 4

The remaining fraction of primaries with energies of 300 TeV after selecting 90% or 50% of the proton or iron showers with cuts in $\mathcal{P}(p)$ or $\mathcal{P}(\text{Fe})$.

Primary	Sel. 90% p	Sel. 50% p	Sel. 90% Fe	Sel. 50% Fe
Proton	90%	50%	8%	<1%
Helium	80%	17%	12%	1.5%
Oxygen	43%	3%	60%	24%
Iron	5%	<1%	90%	50%

9 Systematic Uncertainties

Studies of systematic effects related to the CORSIKA code in its version 4.01, the influence of atmospheric transmission as well as the influence of different theoretical models on the method described so far are addressed very briefly.

Effects related to CORSIKA 4.01

After nearly finishing the simulations used for the studies presented here it was noticed that the EGS stepwidth used in CORSIKA4.01 is too large for simulations including Cherenkov light. This results in a too narrow lateral Cherenkov light distribution and a small overestimation of the total amount of the Cherenkov light [17]. Unfortunately the available CPU power was not sufficient to recalculate the whole MC library. However new simulations with the correct stepwidth only revealed small differences. Especially the presented method itself does not change in principle, only some parameterizations have to be adopted. This also holds for different atmospheric models which were used to simulate the Cherenkov light emission. Detailed comparisons of atmospheric models can be found in [18]. If a realistic atmospheric transmission of the Cherenkov light and a spectral response of the detectors are included in the simulations (which has not been done up to now to focus on the shower development in the atmosphere and because the detector efficiencies may vary for different experiments) the presented method does not have to be altered principally. One only has to account for the zenith angle dependent detection efficiency of the Cherenkov light.

9.1 Theoretical Uncertainties

Theoretical uncertainties concerning the high energy interactions of primary cosmic rays in the atmosphere on the method to determine the primary composition and energy spectrum of CR are summarized into two categories: first the fragmentation of the primary nucleus and afterwards different simulation models of high energy interactions are discussed.

Maximal versus minimal Fragmentation

To generate the showers discussed up to now the “maximal fragmentation” approach to model the remnant of the primary nucleus (consisting of the non interacting nucleons) was used: after the first interaction the nucleus fragments completely into independent nucleons. The shower maximum is reached earlier if “minimal fragmentation” (the noninteracting nucleons of the primary particle proceed as one nucleus further down the atmosphere) is used instead, because the cross section of a complex nucleus is larger than that of a single nucleon. The mean position of the maximum rises by $22 \pm 7 \text{ g/cm}^2$ for 1 PeV iron showers. As the cross sections remain roughly constant with energy this shift is not expected to change drastically in the energy range covered by this paper. Extrapolating the results for iron to oxygen and helium with a simple geometrical parameterization yield expected shifts of 16 and 4 g/cm^2 respectively. In addition to the shift also the spread (RMS) of the position of the shower maximum rises slightly if minimal fragmentation is used. Only small differences in the shape of the longitudinal shower development were found not measurable with a HEGRA like detector. The shift of the shower maximum positions for iron induced EAS results in overestimations of the reconstructed energy by 20% and of $\log_{10}(A)$ by 0.4 if parameterizations achieved from simulations with “maximal fragmentation” are applied to “minimal fragmentation” events. The overestimation of $\log_{10}(A)$ should be measurable with a HEGRA type of detector. In reference [19] the authors conclude that above an energy per nucleon of 2 GeV the fragmentation remains scale invariant. Therefore a measurement of $\log_{10}(A)$ for heavy primaries well below the “knee” (where the results of ground based measurements of the chemical composition can be compared to balloon experiments) will be sufficient to infer the fragmentation mechanism realized in nature.

Different Interaction Models

It goes beyond the scope of this paper to review all different theoretical approaches to model high energy interactions. Instead a comparison of simulations with different interaction models which was performed by the COR-

SIKA authors using the models DPMJET-II, HDPM, QGSJET, SIBYLL and VENUS [3] and kindly passed to the author [20] was analyzed regarding the sensitivity of the presented methods. These simulations do not include the emission of Cherenkov light. Therefore the procedure to reconstruct the primary energy and mass could not be applied directly, but other shower characteristics important for the described methods had to be tested. These were the depth of the shower maxima and elongation rates, the shape of the longitudinal shower development, the shower size at the maximum and the lateral shower development. Please contact the author for details of the comparisons. All the different models of high energy interactions in the atmosphere do not show drastic differences concerning the shower characteristics used in the method described in this paper. This is in contrast to observables related to the hadronic part of EAS. At least up to 1 PeV an exploration of the chemical composition and the energy spectrum can be performed in a nearly model independent manner, if only observables related to the electromagnetic shower part are used. Further studies are needed and currently underway to investigate model differences in the energy region of the knee and beyond.

10 Summary and Conclusions

In this paper methods were presented to determine energy and mass of primary cosmic rays from ground based observations of the electromagnetic cascade of air showers. From the slope of the lateral Cherenkov light density in the range of 20 to 100 m core distance the position of the shower maximum can be inferred without knowledge of the nucleon number of the primary particle. This leads to an unbiased determination of the energy per nucleon and, combined with the shower size at detector level or the number of registered Cherenkov photons, to a measurement of the primary energy. Thus a measurement of the energy spectrum and a coarse determination of the chemical composition are possible without any a priori hypotheses. With the observables considered in the present paper the energy resolution for primary nuclei is limited to approximately 30% at 300 TeV improving to 10% at 5 PeV due to natural fluctuations in the shower development. Further improvements of these results are only possible if accurate measurements of the non electromagnetic components of EAS are added.

At energies below 1 PeV, where results from EAS measurements can be compared to direct data from balloon flights, the determination of the CR mass composition from the analysis of Cherenkov light and particles at detector level of EAS can be substantially improved by combining the results related to the longitudinal shower development with parameters derived from the lateral extension. This allows for detailed tests of the described method to determine the chemical composition and the energy spectrum of cosmic rays.

The main characteristic of the methods presented here is, that it are mainly the longitudinal shower development behind the shower maximum, the number of particles at the maximum and the penetration depth of the shower until it reaches the maximum (both mean value and fluctuations), which determine the results. While the first two items do not vary much for different models describing the development of air showers the last item is more model dependent. In order to achieve results being as model independent as possible it is very desirable to combine the method described in this paper with complementary measurements. Analyses of the early stage of the shower development, of the hadronic and muonic components of EAS or detailed studies of the shower core may be considered for this purpose.

The reconstruction of the air shower parameters as discussed in this paper can be applied also to separate photon and nucleon induced EAS and to reconstruct the primary energy of photons with a much better precision than for primary nuclei. This will be described in a forthcoming paper.

Acknowledgements

The author would like to thank the HEGRA members for their collaboration. Especially I am very grateful to V. Hausteine, who performed most of the MC simulations and determined the chemical composition of CR with a different technique, to G. Heinzemann for many detailed, constructive proposals and improvements as well as for his general support, and to R. Plaga, who pioneered the analysis of charged CR in the HEGRA collaboration, for motivations and detailed discussions. Special thanks to the authors of CORSIKA for supplying us with the simulation program and their support. I thank Gerald Lopez for his careful reading of the text and for providing valuable suggestions. This work was supported by the BMBF (Germany) under contract number 05 2HH 264.

References

- [1] Drury, L.O'C., Rep.Prog.Phys.**46**, 973 (1983)
Blanford, R.D., Eichler, D., Phys.Rep.**154**, 1 (1987)
- [2] Hillas, A.M., Ann.Rev.Astron.Astrophys.**22**, 425 (1984)
Völk, H.J., Proc. of the 20th ICRC Moscow **7**, 157 (1987)
Cesarsky, C.J., Nucl.Phys.B (Proc.Suppl)**28B**, 51 (1992)
Bierman, P.L., 23th ICRC Calagary, Inv. , Rapp. and Highl. Pap., 45 (1993)
Biermann, P.L., Astron.Astrophys.**271**, 649 (1993)
Stanev, T., Biermann, P.L., Gaisser, T.K., Astron.Astrophys.**274**, 902 (1993)
Drury, L.O'C., Aharonian, F., Völk H.J., Astron.Astrophys.**287**, 959 (1994)

- [3] Knapp, J., Heck, D., Schatz, G., FZKA Report **5828** (1997), and references therein.
- [4] Gaisser, T.K., Nucl. Phys. **B** (Proc. Suppl.) **52B**, 10 (1997)
- [5] Wdowczyk, W., J.Phys. **G20**, 1001 (1994)
Kalmykov, N.N., Khristiansen, G.B., J.Phys. **G21**, 1279 (1995) Watson. A.A., Rapp. Talk 25th ICRC Durban (1997)
- [6] Klages, H.O., et al. (KASCADE-Collab.), Nucl. Phys. **B** (Proc. Suppl.) **52B**, 92 (1997)
Kampert, K.-H., et al. (KASCADE-Collab.), astro-ph/9703182 (1997)
- [7] Karle, A., et al. (HEGRA-Collab.), Astropart.Phys. **3**, 321 (1995)
Krawczynski, A., et al. (HEGRA-Collab.), NIM **A383**, 431 (1996)
Lindner, A., et al. (HEGRA-Collab.), Proc. of the 25th ICRC Durban **5**, 113 (1997)
- [8] Aharonian, F., Heinzlmann, G., Proc. of the 15th ECRS, Perpignan (1996), in press (similar in astro-ph/9702059)
- [9] Lindner, A., et al. (HEGRA-Collab.), Talk at the 24th ICRC, Rome (1995), unpublished
Cortina, J., et al. (HEGRA-Collab.), Proc. of the 25th ICRC Durban **4**, 69(1997)
- [10] Plaga, R., et al. (HEGRA-Collab.), Proc. of the 24th ICRC Rome **2**, 693 (1995)
- [11] Protheroe, R.J., Turver, K.E., Nuovo.Cim. **51A**, 277 (1979)
Chantler, M.P., et al. J.Phys. **G8**, L51 (1982)
Turver, K.E., Nucl.Phys.B (Proc.Suppl.) **28B**, 16 (1992)
Kalmykov, N.N., Khristiansen, G.B., Prosin, V.V., Phys.At.Nucl. **58**, 1563 (1995)
- [12] Kamata, K., Nishimura, J., Prog.Theor.Phys., Suppl. **6**, 93 (1958)
Greisen, K. Ann.Rev.Nucl.Sci.**10**,63 (1960)
- [13] Capdevielle, J.N. et al., KFK Report **4998** (1992)
Knapp, J., Heck, D., KFK Report **5196B** (1993)
- [14] Hausteijn, V., doctoral thesis at Univ. of Hamburg (1996)
- [15] Patterson, J.R., Hillas, A.M., J.Phys. **G9**,1433 (1983)
- [16] Gabriel, T.A., et al., Nucl.Instrum.Meth. **A338**,336 (1994)
- [17] Heck, D., private communication
- [18] Horns, D. diploma thesis, Univ. of Hamburg (1997)
- [19] Kalmykov, N.N. and Ostapchenko, S.S., Phys.At.Nucl. **56**, 346 (1993)
- [20] Heck, D., private communication